Terahertz Sources Based on Intracavity Parametric Down-Conversion in Quasi-Phase-Matched Gallium Arsenide

Joseph E. Schaar, Konstantin L. Vodopyanov, Paulina S. Kuo, Martin M. Fejer, *Member, IEEE*, Xiaojun Yu, Angie Lin, James S. Harris, *Fellow, IEEE*, David Bliss, Candace Lynch, Vladimir G. Kozlov, and Walter Hurlbut

Abstract—We have efficiently generated tunable terahertz (THz) radiation using intracavity parametric down-conversion in gallium arsenide (GaAs). We used three types of microstructured GaAs to quasi-phase-match the interaction: optically contacted, orientation-patterned, and diffusion-bonded GaAs. The GaAs was placed in an optical parametric oscillator (OPO) cavity, and the THz wave was generated by difference-frequency mixing between the OPO signal and idler waves. The OPO used type-II phase-matched periodically poled lithium niobate as a gain medium and was synchronously pumped by a mode-locked laser at 1064 nm (7 ps and 200 nJ at 50 MHz). With center frequencies spanning 0.4–3.5 THz, 250-GHz bandwidth radiation was generated. We measured two orders of optical cascading generated by the mixing of optical and THz waves. In a doubly resonant oscillator (DRO) configuration, the efficiency increased by 21× over the singly resonant oscillator performance with an optical-to-THz efficiency of 10^{-4} and average THz power of 1 mW. The GaAs stabilized the DRO by a thermooptic feedback mechanism that created a quasi-continuous-wave train of THz pulses.

Index Terms—Difference-frequency mixing, doubly resonant, gallium arsenide (GaAs), nearly degenerate, optical parametric oscillator (OPO), parametric down-conversion, self-stabilized, terahertz (THz), tunable.

I. INTRODUCTION

TERAHERTZ (THz) waves are potentially useful for numerous applications including real-time imaging and rotational–vibrational spectroscopy, both in condensed and gaseous phases [1], [2]. Parametric down-conversion of optical pulses is an established, but so far inefficient, method for generating THz radiation. Potentially, it enables compact tunable THz

emitters working at room temperature, by using efficient solid state or fiber laser sources with different temporal formats: from continuous wave (CW) to femtosecond pulses. This technique can generate THz radiation using difference frequency generation (DFG) with two laser input beams [3]–[8] or through THz wave parametric oscillation [9]–[11] with a single fixed-frequency optical pump. Alternatively, broadband THz transients can be generated by means of optical rectification (OR) of ultrashort (typically femtosecond) laser pulses [12]–[15].

There are three significant factors that limit THz conversion efficiency in both OR and DFG, namely: 1) conventional crystals used for THz generation (e.g., $LiNbO_3$ and ZnTe) have large absorption at THz frequencies (characteristically 10–100 cm^{-1} [16], [17], 2) there is a mismatch between propagation velocities of the THz wave and the optical pulse that limits (especially for OR) the useful length of the crystal, and 3) a large quantum defect. Optical-to-THz conversion efficiencies achieved so far are low [18], typically 10^{-6}–10^{-9}, even with femtosecond pump pulse energies as high as 10 mJ [19]. A way to solve the problem of propagation velocity mismatch and increase the interaction length is to use tilted pulse front excitation. A conversion efficiency of 5×10^{-4} and a THz average power of 240 μW was reported in [15] using bulk lithium niobate pumped by optical pulses from a 1 kHz Ti:Sapphire oscillator–regenerative amplifier system with 500 mW of average power. Another approach to increase the efficiency of OR is to use quasi-phase-matched (QPM) nonlinear materials, as was first demonstrated with periodically poled lithium niobate (PPLN) [13], [20]. The effective mixing length is increased due to quasi-phase-matching allowing for looser pump focusing, reducing the magnitude of parasitic nonlinear effects for a given pump pulse energy. The authors of [13] and [20] used femtosecond pulses at 800 nm and a PPLN crystal with multiple QPM periods and achieved a conversion efficiency $\sim 10^{-5}$. The PPLN crystal was cryogenically cooled ($T = 18$ K) to reduce THz absorption.

More recently, THz wave generation was demonstrated in QPM-GaP [8] and QPM gallium arsenide (GaAs) [21], [22]. III–V semiconductors are attractive for QPM THz wave generation because of several properties, including: 1) a small THz absorption coefficient [smaller by more than one order of magnitude than commonly used electrooptic (EO) crystals: $LiNbO_3$, ZnTe, CdTe, and ZnSe] [16], [17], [23], [24], 2) a large nonlinear coefficient, and 3) a large coherence length due to a small mismatch between the optical group and THz phase velocities.

In [8], THz waves were generated by DFG in a periodically inverted GaP wafer stack, which was pumped with 10 ns pulses near 1.55 μm. The authors of [21] produced THz radiation via OR using femtosecond laser pulses and two different QPM-GaAs structures: 1) diffusion-bonded GaAs (DB-GaAs) [25] and 2) orientation-patterned GaAs (OP-GaAs) [26]. By changing the GaAs QPM period (504–1277 μm), or the pump wavelength (2–4.4 μm), tunable (0.9–3 THz) output was achieved with up to 3.3% quantum conversion efficiency with 2.3 μJ of pump pulse energy. With a Tm-fiber laser pump source at $\lambda \approx 2$ μm, 3 μW of average THz power was generated in an OP-GaAs crystal at 1.8 and 2.5 THz [22].

Here we report THz generation using intracavity DFG in a picosecond pulse optical parametric oscillator (OPO). This paper focuses on experimental results. A detailed theoretical analysis will be given in a subsequent paper.

II. THZ WAVE GENERATION USING PICOSECOND OPO PULSES

A. Picosecond Pulse DFG in QPM-GaAs

Detailed analysis of the generation of THz pulses by plane wave QPM-DFG [27] with transform-limited pump pulses shows that, for a given crystal length, QPM period, and pump pulse energy, there is a characteristic pulse duration τ_{nom} below which the efficiency reaches an asymptotic value, and above which the efficiency decreases monotonically. This characteristic pulse duration corresponds to a bandwidth that matches the acceptance bandwidth of the DFG process, and the conversion efficiency for this pulse length is 70% of the asymptotic value reached for shorter pulses.

For Gaussian pump beams, the efficiency rises only slowly for focusing tighter than confocal for THz radiation [27]. For this focusing condition and a pulse duration of τ_{nom}, the bandwidth of the THz radiation decreases with crystal length, while the efficiency for a fixed pulse energy does not change (until the crystal length becomes comparable to the THz absorption length). As peak pump intensities are often limited by parasitic nonlinear effects (two- and three-photon absorption, nonlinear refraction), the lower intensities associated with the looser focusing in longer crystals can be advantageous in practical implementations.

Under these pulse length and focusing conditions, the THz pulse energy scales with the product of the energies of the picosecond optical pulses, $U_{THz} = \eta U_1 U_2$. As a numerical example of generating 1.5 THz radiation using DFG of 2.1 μm pulses in a 1-cm-long GaAs crystal ($\tau_{1,2} = \tau_{nom} = 3.4$ ps), the efficiency η is 3.4×10^{-4} per microjoule of optical pulse energy. For 200 nJ pulse energies in both optical waves (10 W each, 50 MHz), this corresponds to a THz pulse energy of 13.5 pJ (0.67 mW).

Using picosecond pulses, which match the bandwidth in QPM-GaAs for crystals of length equal to a THz absorption length, at optical frequencies to pump QPM-GaAs in a single-pass DFG process can create a milliwatt-level THz source with a large optical-to-THz conversion per microjoule of pump pulse energy while limiting higher order nonlinear effects that would become increasingly important at shorter pulse widths.
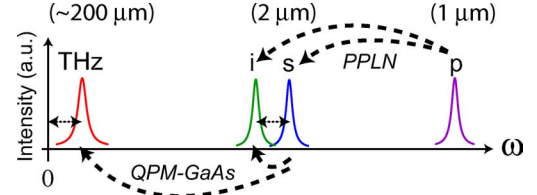

Fig. 1. Frequency-domain schematic of the four waves involved in THz generation (pump, signal, idler, and THz, not drawn to scale). The pump wavelength is near 1 μm, and the signal and idler wavelengths are near 2 μm.

B. Picosecond Pulse OPO

Our approach in generating THz radiation is based on the DFG inside a QPM GaAs crystal between the picosecond signal and idler pulses of a low-loss synchronously pumped OPO. Either extra- or intracavity mixing in GaAs can be performed. A low-loss OPO cavity has large circulating peak powers that can significantly increase the optical-to-THz conversion efficiency for intracavity experiments. This intracavity enhancement scheme has previously been used for intracavity sum-frequency generation and DFG in the visible and mid-infrared frequency ranges [28], [29].

In our experiments, the OPO gain crystal, PPLN, is pumped by a mode-locked $\sim$7 ps pulse width laser with a wavelength near 1 μm. In the PPLN crystal (see Fig. 1), energy is transferred from the pump to the signal and idler waves ($\omega_i < \omega_s < \omega_p$ where i, s, and p refer to the idler, signal, and pump, respectively) that have frequencies symmetrically split about the degenerate frequency, $\omega_p/2$ ($\lambda \sim 2$ μm). By changing the temperature of the PPLN crystal, the signal and idler frequencies can be tuned symmetrically about degeneracy. The frequency spacing between the signal and idler is equal to the THz frequency that will be generated in a DFG process ($\omega_{THz} = \omega_s - \omega_i$). The OPO uses type-II (o–oe) phase-matching that allows narrow OPO signal and idler spectral widths while operating near degeneracy, and consequently, generating a THz wave with a full-width at half-maximum (FWHM) bandwidth $\sim$200 GHz. The signal and idler fields are linearly orthogonally polarized. In the QPM-GaAs crystal, energy flows from the signal wave to the idler and THz waves. Changing the center frequency of the THz wave involves: 1) changing the temperature of the PPLN crystal to tune ω_{THz} and 2) using the correct GaAs grating period to provide the necessary phase-matching between the signal, idler, and THz waves.

C. QPM-GaAs Samples

GaAs has many attractive properties for THz generation such as a small THz absorption coefficient, small mismatch between the optical group index ($n_{g,opt} \approx 3.41$ [30]) and THz phase index ($n_{THz} \approx 3.6$ [31]), large thermal conductivity, large nonlinear coefficient, and well-established QPM fabrication techniques. The absorption in GaAs is <4.5 cm^{-1} for $\nu < 3$ THz, and $\sim$1 cm^{-1} at 1.5 THz [32]. The large thermal conductivity of GaAs, 52 W/m·K [33], reduces temperature changes and thermooptic index perturbations at large average pump powers. The
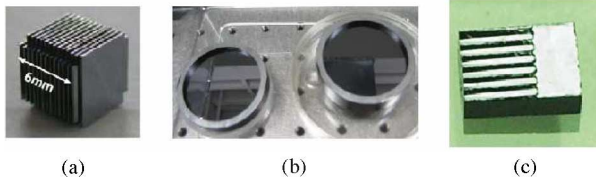
Fig. 2.   (a) DB-GaAs with dimensions 10 mm×10 mm×6.05 mm and QPM period of 504 μm. (b) OC-GaAs with diameters of 5.08 cm and QPM periods of 2 mm. (c) OP-GaAs with thickness of ∼800 μm, width of 6 mm, length of 5 mm, and QPM period of 704 μm.

nonlinear coefficient for THz generation from DFG between two optical waves is $d_{14} = 47$ pm/V [27].

The periodic structure needed for quasi-phase-matching cannot be achieved in GaAs by ferroelectric poling, as is commonly done in ferroelectric crystals such as LiNbO$_3$. GaAs is a cubic crystal with $\overline{4}3$m symmetry, whose linear properties are isotropic, and in which 90° rotations around the ⟨100⟩ axes result in a crystallographic inversion, and hence, a sign change of the nonlinear susceptibility. The nonzero elements of the GaAs nonlinear coefficient tensor are d_{xyz} and its permutations.

We used three different types of microstructured GaAs: DB-GaAs [25], optically contacted GaAs (OC-GaAs), and OP-GaAs [26]. DB-GaAs samples are made of N individual GaAs plates by rotating every other plate by 180° about [110] to create a sample with $N/2$ QPM periods. The GaAs plates are brought together under pressure and high temperature that allows diffusion to occur across the interface creating a nearly monolithic structure. The DB-GaAs sample we used for THz generation had an aperture of 10 mm × 10 mm, length of 6.05 mm, QPM period of 504 μm, and was constructed of 24 GaAs plates [see Fig. 2(a)].

OC-GaAs construction also involves separate [110] wafers of GaAs that are brought together with a 180° rotation about [110] between neighboring wafers. The wafers, however, are not heated to create a monolithic crystalline structure. They are contacted creating an interface that is maintained by van der Waals interactions [see Fig. 2(b)]. The thickness of the GaAs wafers used to fabricate the stacks used in these experiments ranged from 0.5 to 1.0 mm. The OC-GaAs samples have lower infrared losses over larger useful apertures than the DB-GaAs sample.

OP-GaAs is the third type of microstructured QPM-GaAs [see Fig. 2(c)]. OP-GaAs is manufactured using photolithography and molecular beam epitaxy to grow a thin-film template with periodic crystal inversions. A thick film (∼1 mm) is then grown on the template by hydride vapor phase epitaxy (HVPE) to produce bulk OP-GaAs [26]. The QPM period of OP-GaAs is easily controlled down to tens of microns, and it can be maintained with good long-range order for lengths greater than the 1-cm-long samples required for THz generation since they are fabricated with a photolithographic process.

Recently, 15-wafer-thick OC-GaAs samples have been produced with a useful aperture of 3 mm × 3 mm and infrared losses of ∼0.01 cm^{-1}. OP-GaAs samples now grown in a single HVPE step are ∼1 mm in thickness [34] with 2 μm absorption <0.005 cm^{-1} [35].
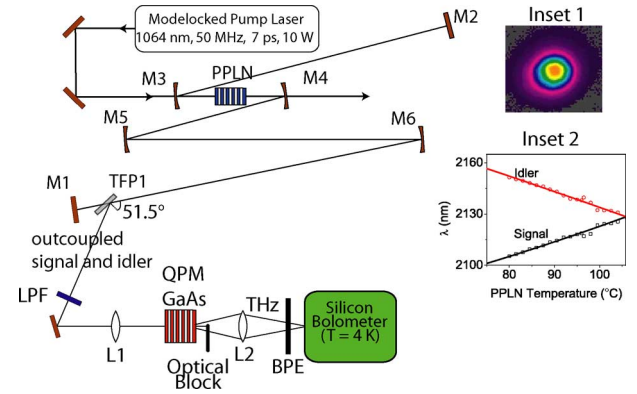

Fig. 3.   Schematic of SRO and extracavity DFG experiment. The signal and idler were outcoupled from the SRO and focused into various QPM-GaAs samples. L1 was a focusing lens for the signal and idler, and L2 was a Picarin lens that focused the THz beam onto the liquid-helium-cooled silicon bolometer. Inset 1: signal TEM$_{00}$ resonating spatial mode profile with $M^2 = 1.2$. Inset 2: type-II PPLN temperature-tuning curves for both the o–wave signal and e–wave idler (measured data points and solid-line polynomial fits).

III. SRO EXTRACAVITY THz GENERATION

Fig. 3 shows the experimental setup for THz generation outside the cavity of the synchronously pumped singly resonant OPO [singly resonant oscillator (SRO)]. The OPO pump laser was a Nd:YVO$_4$ CW-mode-locked solid-state laser (*pico*TRAIN, High Q Laser) with a 50 MHz pulse repetition rate, 7 ps Gaussian FWHM intensity pulse width, 1064 nm wavelength, and 10 W average output power. The linear SRO cavity was 3 m long with a round-trip time equal to the period between pump laser pulses. For the OPO gain medium, we used an antireflection (AR) coated (for pump, signal, and idler) MgO-doped type-II PPLN crystal, with a QPM period of 14.1 μm and length of 10 mm. The nonlinear optical coefficient for type-II quasi-phase-matching at 2.1 μm, $d_{31,\mathrm{eff}} = (2/\pi)d_{31} = 2.35$ pm/V calculated from [36] at 1.06 μm and scaled using Miller's rule [37] to 2.1 μm, was 6.2× smaller than the coefficient for typical type-0 (e-ee) quasi-phase-matching ($d_{33,\mathrm{eff}}$), which resulted in an OPO parametric gain reduced by a factor of 38.4 compared to the usual type-0 configuration. The focused 1 μm laser spot size ($1/e^2$ intensity radius) at the center of the PPLN was 30 μm. Mirrors M1 and M2 were end mirrors for the resonating signal wave. Mirrors M3 and M4 were separated by 21.3 cm and had 20 cm radii of curvature that created a signal spot size of 57 μm in the center of the PPLN. A second position for focused signal and idler beams (140 μm beam waist) was created using mirrors M5 and M6, which were separated by 50 cm and had 50 cm radii of curvature. This second focus is important for intracavity THz generation and will be discussed in Section IV. The distance between mirrors M4 and M5 was 30 cm, and the remaining cavity length of ∼200 cm was divided evenly into the two end lengths (M6–M1 = M3–M2). All mirrors were AR-coated for the pump and high-reflectivity (HR) coated for the signal and idler waves with a reflection loss <0.1%. The front surface of the thin-film polarizer, TFP1, was AR-coated for signal (p-polarization) transmission and HR-coated for idler (s-polarization) reflection (p-polarization

incident on the polarizer is equivalent to an *o*-wave in the PPLN crystal). Fig. 3 (inset 1) shows the signal's TEM_{00} spatial mode measured by a pyroelectric-array camera. The beam M^2 parameter was 1.2 as measured by focusing the 2.1 μm beam outside the cavity. The type-II QPM temperature-tuning curve for the signal and idler wavelengths is shown in Fig. 3 (inset 2) [38].

Large powers at both signal and idler wavelengths are required for extracavity THz DFG. The nominal polarizer angle of incidence of 55° minimized the signal-SRO threshold but did not outcouple the signal wave for extracavity experiments. We chose the polarizer angle of 51.5° to increase the signal outcoupling without greatly reducing the OPO quantum conversion efficiency. The signal and idler reflectivities at the polarizer were 2% and 99.2%, respectively. The cavity mirrors and PPLN surfaces created 2.4% round-trip loss, and the round-trip losses of the polarizer were 4% (total OPO round-trip loss of 6.4%). We measured a signal autocorrelation width of 8.5 ps corresponding to a signal pulse width of 6 ps, assuming a transform-limited Gaussian pulse. A longpass filter ($\lambda > 1.9$ μm) blocked the unwanted near-infrared and visible-wavelength light. At a PPLN temperature of 86°C, the signal and idler average powers were 620 and 180 mW, respectively. The powers varied only slightly with the temperature of the PPLN crystal. L1 focused the signal and idler beams down to 80 μm at the center of the QPM-GaAs crystal. The signal field was linearly polarized along the GaAs [001] direction, and the idler and THz fields were polarized along [110]. All beams propagated along [1$\bar{1}$0]. THz radiation was generated via picosecond DFG inside the QPM-GaAs sample. The optical beams were blocked by a small metal wire located directly after the GaAs crystal. The majority of the THz wave propagated beyond the metal wire, because the THz diffraction cone was ~100× larger than that of the optical beam. The THz radiation was focused by a Picarin lens (L2, THz transmission ~40%) onto a cryogenically cooled silicon bolometer ($T = 4$ K). A black polyethylene filter (0.8 mm thick) was placed directly before the bolometer and blocked any remaining IR and visible light.

Fig. 4 shows measured THz center frequencies $\nu_{\rm THz}$ versus QPM period for several OP-, OC-, and DB-GaAs crystals [39]. They are in good agreement with $\nu_{\rm THz} = c/(\Delta n \Lambda_g)$, where Λ_g is the QPM-grating period and $\Delta n = n_{\rm THz} - n_{\rm g,opt}$ [27]. Dispersion information from [30] and [31] was used for GaAs at near-IR and THz frequencies, respectively. Typical generated THz average powers were between 0.1 and 1 μW.

IV. SRO INTRACAVITY THz GENERATION

A. SRO Intracavity THz Generation

The QPM-GaAs samples were placed inside the SRO cavity to increase the generated THz average powers. The angle of incidence on the intracavity polarizer was set to 55° which reduced the polarizer losses to 0.1%. We expect the GaAs nonlinear refraction, and consequently, Kerr lensing to place an upper limit on the circulating intensity in the OPO. The Gaussian spatial intensity profile of the signal and idler beams will create a Gaussian transverse phase, and the quadratic component will
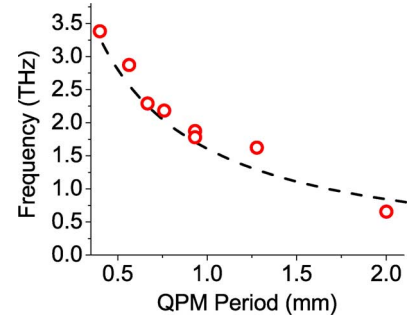

Fig. 4. THz center frequencies versus GaAs QPM period (data points) for OC-, OP-, and DB-GaAs samples in good agreement with theory (dashed line) using dispersion information from [30] and [31] for GaAs at near-IR and THz frequencies, respectively.
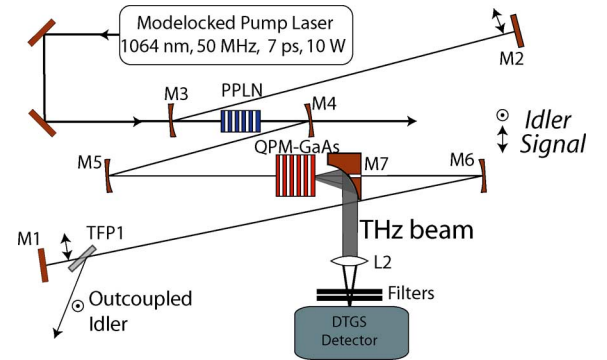

Fig. 5. Schematic of measurements of THz average powers generated via intracavity DFG in the SRO configuration. The THz beam was outcoupled by M7, focused by Picarin lens L2, and measured with a DTGS pyroelectric detector.

cause signal and idler focusing in the GaAs. An effective focal length can be calculated from the curvature of the transverse phase profile including both self- and cross-phase modulation terms, and the GaAs can be modeled as a dynamic nonlinear lens with a lens strength proportional to intracavity intensity. It is possible to design the OPO cavity with minimum sensitivity to the Kerr lensing at the location of the GaAs crystal, to allow oscillation at large intracavity powers. Similar designs have been applied to mode-locked laser cavities that have a thermally loaded diode-pumped gain element.

We designed the cavity to produce a focused 140 μm spot size for the signal and idler beams at a position roughly halfway between M5 and M6 (see Fig. 5). Following a design approach similar to that in [40], we placed the GaAs in this focus where the signal and idler intensities as well as optical-to-THz conversion efficiency were large. For this spot size and GaAs-crystal length of 1 cm, the 3-m-long OPO can maintain oscillation from startup down to focal lengths of $f_{\rm Kerr} \approx 2$–4 cm. When $f_{\rm Kerr} \sim L_{\rm GaAs}$, the GaAs thin lens approximation breaks down, and a more general analysis is required.

The THz wave was extracted from the SRO by mirror M7, which was a gold-coated 90°-off-axis parabolic mirror with a focal length of 5 cm placed ~5 cm after the QPM-GaAs crystal, which created a well-collimated THz beam. A 3-mm-diameter
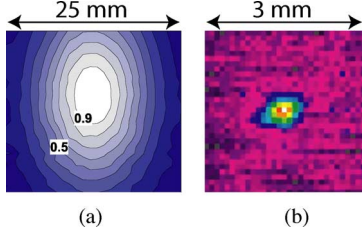
Fig. 6. (a) Collimated THz beam intensity profile reconstructed from scanning knife-edge measurements just before lens L2. (b) Focused ($f = 5$ cm) THz beam intensity profile measured by a pyroelectric camera (1 pixel $= 100 \mu$m $\times 100 \mu$m) 5 cm after L2.

hole was drilled through M7 to fully transmit the resonating signal wave. The visible and IR radiation was blocked by two polyethylene filters that transmitted >45% for $\nu < 3$ THz. For a 100 μm THz spot size generated in the GaAs (product of signal and idler Gaussian 140 μm spots), the 1 inch aperture gold parabolic mirror collected >90% of the incident power at frequencies >2.8 THz.

The DB-GaAs sample (6 mm long and QPM period of 504 μm) generated THz radiation with a center frequency of 2.8 THz and FWHM spectral bandwidth estimated to be ∼250 GHz from the convolution of the measured 200 GHz bandwidths of the signal and idler waves [38] and limited to 250 GHz by the QPM-GaAs acceptance bandwidth [27]. The measured THz average power was 50 μW (after M7), and the measured intracavity powers of the signal and idler were 11.1 W and 2.2 W, respectively, with a large signal power enhancement compared to 690 mW in the previous section (before the longpass filter). For a given pump depletion, the signal power enhancement A is

$$A = \frac{a_{\text{ext}}}{a_{\text{int}} R} \qquad (1)$$

where $a_{\text{ext}} = 6.4\%$ was the round-trip loss for extracavity experiments with signal output coupling $R = 2\%$ and $a_{\text{int}} = 14.4\%$ was the round-trip loss for the intracavity experiments. The DB-GaAs roundtrip loss was 12%. The calculated enhancement of $A = 22$ is close to the measured value of 11.1 W/0.69 W = 16. The idler power of 2.2 W agreed with the quantum defect of 0.5 (pump to idler) and the measured 50% depletion of 8.9 W of pump power. The undepleted pump power was measured after M4 (see Fig. 5). The optical-to-THz conversion efficiency was 5.6×10^{-6} (quantum efficiency of 5.6×10^{-4}).

Fig. 6(a) shows the THz beam intensity profile after collimating mirror M7, reconstructed from scanning knife-edge measurements. The horizontal and vertical $1/e^2$ spot sizes were 7.8 and 13.3 mm, respectively. The THz beam 5 cm after THz lens L2 ($f = 5$ cm) was captured [see Fig. 6(b)] by a pyroelectric-array camera [38] and was ∼2 pixels in width (1 pixel $= 100 \mu$m $\times 100 \mu$m). Taking the input beam size from the knife-edge measurements, the focused spot size agreed with the theoretical diffraction-limited spot size of 160 μm. The polarization of the THz beam was along the [110] GaAs crystalline direction, in agreement with the symmetry of the GaAs $\chi^{(2)}$ tensor [41], and for signal and idler fields polarized along the [001] and [110] directions, respectively.
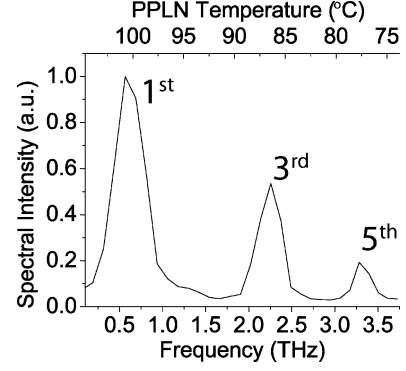

Fig. 7. First-, third-, and fifth-order QPM with a 4-mm-long OC-GaAs crystal with $\Lambda_g = 2$ mm allowing generation of three different THz center frequencies (0.62, 2.24, and 3.32 THz, respectively) with a single QPM-GaAs sample.

B. Higher Order QPM THz Generation

The two-step down-conversion process (1 μm $\rightarrow$ 2 μm $\rightarrow$ 200 μm) by which we generate THz radiation requires operating the OPO very close to degeneracy. For generating 2.8 THz radiation, the signal and idler wavelength separation is 42 nm at an average wavelength of 2128 nm. This tuning behavior also allowed generation of other THz frequencies by taking advantage of higher order QPM peaks in the GaAs sample.

Modeling the QPM crystal as having a fundamental spatial frequency of $k_g = 2\pi/\Lambda_g$, and equal length positive and negative half-periods, the mth spatial harmonic of the grating enables quasi-phase-matching when the wavevector mismatch

$$\Delta k = k_s - k_i - k_{\text{THz}} - m k_g \quad (m \text{ odd}) \qquad (2)$$

is zero [42]. Here, $k_j = 2\pi n_j \nu_j / c$ is the wavevector magnitude, n_j is the index of refraction, and ν_j is the frequency. The maximum DFG efficiency occurs for $\Delta k = 0$. Assuming perfect phase-matching ($\Delta k = 0$), nearly degenerate signal and idler ($\nu_s \approx \nu_i \gg \nu_{\text{THz}}$), and negligible THz dispersion ($n_{\text{THz}} \approx$ constant), the THz center frequency scales linearly with m:

$$\nu_{\text{THz}} = m \left(\frac{c}{\Delta n \Lambda_g} \right). \qquad (3)$$

We measured the higher order QPM tuning curves for a 4-mm-long OC-GaAs crystal with $\Lambda_g = 2$ mm. Fig. 7 shows the first-, third-, and fifth-order QPM tuning curves with center frequencies of 0.62, 2.24, and 3.32 THz, respectively. The center frequencies do not scale exactly with m because of the GaAs dispersion between 0.5 and 4.0 THz.

C. Cascading

In a DFG process within the GaAs crystal, the largest energy photon (OPO signal) is destroyed, and two lower energy photons (OPO idler and THz) are generated, i.e., the GaAs crystal parametrically amplifies the OPO idler, depleting the OPO signal and generating a THz photon. Since the ratio of the THz to the optical frequency is ∼1%, 100% depletion of the signal energy would correspond to an optical-to-THz conversion efficiency of only 1%. In order to improve this efficiency, it may be possible to take advantage of a cascading scheme, to generate more than
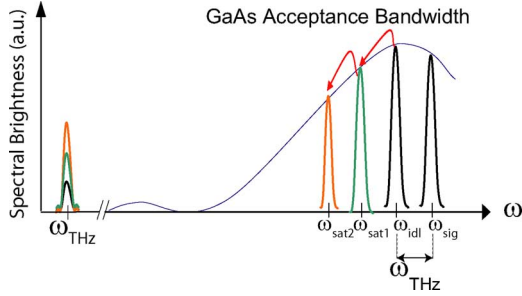
Fig. 8. Parametric down-conversion and cascading illustrating amplification of the THz wave after each cascading process, $\omega_s > \omega_i \gg \omega_{\mathrm{THz}}$.
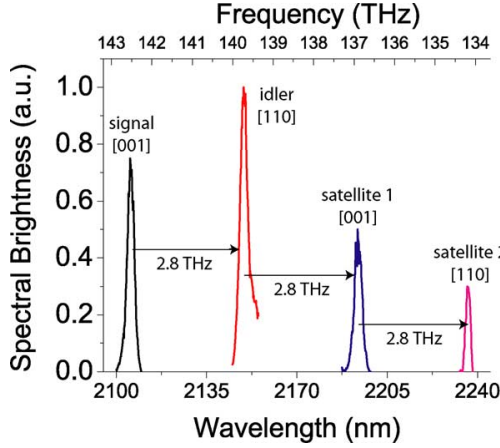

Fig. 9. Measured output spectrum of the SRO with idler wave resonant. The two satellite peaks are generated by cascading of the THz-DFG process. Peaks are labeled with their polarization, referenced to the axes of the GaAs crystal.

Fig. 10. Schematic of the linear DRO with an "offset" cavity design. M1–M8 were cavity mirrors, and M9 was an off-axis parabolic mirror for THz outcoupling.

spectra proved that two cascading events occurred; however, the optical-to-THz conversion efficiency was not significantly improved since the average powers of the two satellites were very small. Having satellite waves with powers comparable to the signal and idler will require all 2 μm waves (signal, idler, and satellites) to be resonant in the optical cavity. A dispersion-compensated cavity designed to obtain such multiply resonant operation is currently under construction.

V. DRO INTRACAVITY THz GENERATION

A. DRO Operation

The THz average power can be increased in a doubly resonant OPO [doubly resonant oscillator (DRO)], in which both the signal and idler are resonant. Fig. 10 shows the DRO setup with the addition of two mirrors, M3 and M4, and a second polarizer, TFP2, to the SRO configuration of Fig. 5. To avoid back conversion of the signal and idler on the return pass through the PPLN [45], we made distances TFP1–M1 and TFP1–M3 unequal. In order to keep the round-trip times for the signal and idler waves equal, the paths TFP2–M2 and TFP2–M4 were correspondingly adjusted. In this "offset" cavity design, the signal and idler pulses overlapped in time during their forward pass through the PPLN; however, they did not overlap on the return pass. Another challenge for DRO operation is the required simultaneous resonance of the signal and idler waves [46], requiring precise control of both cavity lengths.

Both polarizers were set to an angle of 51° that equalized the round-trip losses for the signal and idler waves. The total round-trip loss including DB-GaAs was 22.4% (2.4% from mirrors and PPLN, 12% from DB-GaAs, and 8% from two polarizers). In a first experiment, rather than servo-locking the DRO, we simply scanned one of the cavity mirrors through multiple cavity resonances at a 100 Hz rate and measured bursts of oscillation with a duty cycle of 30%. During these DRO bursts, we generated 1 mW of THz average power at 2.8 THz from 8.5 W with an optical-to-THz efficiency of 1.2×10^{-4} (quantum efficiency of 1.2%) [38], which was an increase of 21× over the SRO results with the DB-GaAs crystal. We found that the generated 1 mW of THz output power was within $\pm 10\%$ of theoretical predictions for intracavity signal and idler

one THz photon for each signal photon destroyed [43], [44]. Fig. 8 illustrates this process. Similar to the parametric amplification mentioned earlier, the OPO idler will amplify the THz wave and generate a down-shifted satellite $\omega_{\mathrm{sat},1}$. This process can be iterated up to a limit set by the phase-matching bandwidth of the QPM-GaAs crystal $\Delta\Omega_{\mathrm{accept,GaAs}}$. Therefore, the number N can be $N \approx \Delta\Omega_{\mathrm{accept,GaAs}}/\omega_{\mathrm{THz}}$.

To explore these effects experimentally, we slightly modified the apparatus shown in Fig. 5. By rotating the polarizer by 90°, the idler rather than the signal was resonant in the SRO. Resonating the idler rather than the signal wave increased the efficiency of generating the first satellite. The temperature of the PPLN crystal was set to 82.3°C to generate signal and idler waves separated by 2.8 THz. A small amount of power in each optical wave leaked out SRO mirror M1 (see Fig. 5) and was characterized with a grating monochromator. The OPO signal, idler, and two satellites were observed around 2100–2240 nm (see Fig. 9). The generated THz output (not shown) was measured by the deuterated triglycine sulfate (DTGS) detector. The grating monochromator was not calibrated for relative power measurements of the four waves shown in Fig. 9; the relative heights of the peaks shown are arbitrary, but indicate the ordering of the strengths of the waves. Consistent with expectations, the separation between adjacent peaks was 2.8 THz, and adjacent fields were orthogonally polarized. The measured
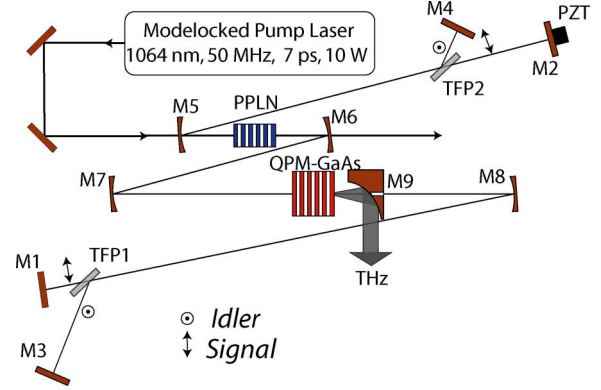
powers of 10.2 and 17 W, respectively, and efficiency following the theory described in Section II-A. The resonant enhancement for both waves was low, because the round-trip losses were >20%. Later, we achieved quasi-CW DRO operation using electronic feedback (piezoelectric stack attached to one end mirror) or a passive thermooptic feedback mechanism described in the next section.

B. Thermooptic DRO Self-Stabilization

An electronic dither-and-lock control system was developed and successfully locked the synchronously pumped DRO to peak resonance where $P_{\max} = P_s + P_i$ (peak of the cavity resonance). With a single 1-mm-thick GaAs wafer in the cavity, the DRO was electronically stabilized with 90 W of average intracavity 2.1 μm power and 84% pump depletion for >30 minutes. Without electronic control but with an 8-mm-long OC-GaAs sample, we observed a self-stabilizing effect that maintained DRO operation for >30 minutes (only terminated due to expansion of the optical table due to temperature changes in the room). This passive thermooptic feedback mechanism provides length–noise suppression, as has been demonstrated in other parametric oscillators using AgGaS$_2$ as the stabilizing element [47].

To understand the origin of the thermooptic stabilization, consider the case where the length of the DRO cavity is slightly longer than the optimum that maximizes $P_{\max}$, so that a decrease in cavity length increases the circulating power. In the presence of a perturbation that decreases the cavity length, there will be an increase in the temperature of the GaAs crystal due to the increase in absorbed power, a positive thermooptic response ($dn/dT > 0$) due to the temperature rise, and a compensating increase in the optical path length. Such a mechanism provides negative feedback with respect to length perturbations. The thermally loaded DRO remains self-stabilized as long as the bandwidth of the length perturbations falls within the unity-gain bandwidth of the thermal self-stabilization process. The thermal bandwidth scales inversely with the thermal diffusion time across the 2.1 μm wavelength beam spot in the GaAs crystal [47]. For the 140 μm spot used in these experiments, this condition corresponds to a bandwidth of 1.8 kHz. The passive feedback does not lock to peak resonance as the dither-and-lock system does. It requires an initial length adjustment to operate near $P_{\max}$. A more detailed theoretical description will appear subsequently.

Fig. 11 shows the 1.5 THz power measured by the DTGS detector (chopped at 10 Hz). The DRO cavity contained an 8-mm-long OC-GaAs sample ($\Lambda_g = 1.07$ mm) that simultaneously generated THz power and stabilized the DRO. Additional electronic feedback can be used in conjunction with the thermooptic self-stabilization to further suppress length perturbations and to lock to a set THz power level.

VI. CONCLUSION AND FUTURE WORK

We demonstrate a novel source of frequency-tunable THz radiation based on intracavity parametric down-conversion in three types of room-temperature QPM-GaAs (OC-, OP-, and DB-GaAs). As a pump for THz generation, we used the sig-
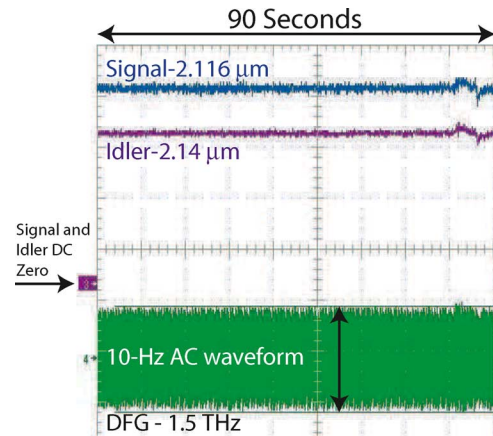

Fig. 11.   Passively self-stabilized DRO signal (2.116 μm), idler (2.14 μm), and signal–idler DFG (1.5 THz radiation chopped at 10 Hz) measured waveforms for a duration of 90 s.

nal and idler waves of picosecond-pulse near-degenerate type-II singly and doubly resonant OPOs. Type-II QPM enabled near-transform-limited pulses with wavelengths near 2.1 μm to be generated close to degeneracy, and the THz center frequency was tunable from 0.4 to 3.5 THz. In both cases of active (electronic feedback) and passive (GaAs thermooptic feedback) stabilization, the DRO operated for >30 minutes with only small fluctuations in output power. Two orders of optical cascading were measured during intracavity THz generation. We have generated 1 mW of THz average power from 180 nJ pump laser pulses with an optical-to-THz conversion efficiency of 1.2×10^{-4} (quantum efficiency of 1.2%).

With total cavity losses of 4%, it should be possible to reach 20 mW of average THz power with a 2.1 μm wavelength spot size of $\sim$350 μm in the GaAs. Experiments are underway with improved polarizers with round-trip losses of 10^{-3} and GaAs samples with losses of 2% to demonstrate this performance. Ring cavity designs offer an approach to a further, reduction of cavity losses.

The output power is potentially scalable to >50 mW by implementing a design with multiple orders of resonant cascading. Such a system would require dispersion compensation, to maintain resonance across the broader infrared spectrum of such a device, and further, reduction of intracavity loss.

REFERENCES

[1] N. Nagai, T. Imai, R. Fukasawa, K. Kato, and K. Yamauchi, "Analysis of the intermolecular interaction of nanocomposites by THz spectroscopy," *Appl. Phys. Lett.*, vol. 85, pp. 4010–4012, 2004.

[2] N. Nagai and Y. Katsurazawa, "Analysis of the inter-molecular interactions between amino acids and acetone by THz spectroscopy," *Wiley Periodicals, Inc.*, vol. 85, pp. 207–213, 2007.

[3] F. Zernike, Jr. and P. R. Berman, "Generation of far infrared as a difference frequency," *Phys. Rev. Lett.*, vol. 15, pp. 999–1002, 1965.

[4] T. J. Bridges and A. R. Strnad, "Submillimeter wave generation by difference-frequency mixing in GaAs," *Appl. Phys. Lett.*, vol. 20, pp. 382–384, 1972.

[5] B. Lax, R. L. Aggarwal, and G. Favrot, "Far-infrared step-tunable coherent radiation source: 70 μm to 2 mm," *Appl. Phys. Lett.*, vol. 23, pp. 679–681, 1973.

[6] W. Shi, Y. J. Ding, N. Fernelius, and K. Vodopyanov, "Efficient, tunable, and coherent 0.18–5.27 THz source based on GaSe crystal," *Opt. Lett.*, vol. 27, pp. 1454–1456, 2002.

[7] Y. Sasaki, Y. Avetisyan, K. Kawase, and H. Ito, "Terahertz-wave surface-emitted difference frequency generation in slantstripe-type periodically poled LiNbO₃ crystal," *Appl. Phys. Lett.*, vol. 81, pp. 3323–3325, 2008.

[8] I. Tomita, H. Suzuki, H. Ito, H. Takenouchi, K. Ajito, R. Rungsawang, and Y. Ueno, "Terahertz-wave generation from quasi-phase-matched GaP for 1.55 μm pumping," *Appl. Phys. Lett.*, vol. 88, pp. 071118-1–071118-3, 2006.

[9] M. A. Piestrup, R. N. Fleming, and R. H. Pantell, "Continuously tunable submillimeter wave source," *Appl. Phys. Lett.*, vol. 26, pp. 418–421, 1975.

[10] K. Kawase, M. Sato, T. Taniuchi, and H. Ito, "Coherent tunable THz-wave generation from LiNbO₃ with monolithic grating coupler," *Appl. Phys. Lett.*, vol. 68, pp. 2483–2485, 1996.

[11] T. J. Edwards, D. Walsh, M. B. Spurr, C. F. Rae, M. H. Dunn, and P. G. Browne, "Compact source of continuously and widely tunable terahertz radiation," *Opt. Exp.*, vol. 14, pp. 1582–1584, 2006.

[12] L. Xu, X.-C. Zhang, and D. H. Auston, "Terahertz beam generation by femtosecond optical pulses in electro-optic materials," *Appl. Phys. Lett.*, vol. 61, pp. 1784–1786, 1992.

[13] Y.-S. Lee, T. Meade, V. Perlin, H. Winful, T. B. Norris, and A. Galvanauskas, "Generation of narrow-band terahertz radiation via optical rectification of femtosecond pulses in periodically poled lithium niobate," *Appl. Phys. Lett.*, vol. 76, pp. 2505–2507, 2000.

[14] C. Weiss, G. Torosyan, Y. Avetisyan, and R. Beigang, "Generation of tunable narrow-band surface-emitted terahertz radiation in periodically poled lithium niobate," *Opt. Lett.*, vol. 26, pp. 563–565, 2001.

[15] A. G. Stepanov, J. Kuhl, I. Z. Kozma, E. Riedle, G. Almasi, and J. Hebling, "Scaling up the energy of THz pulses created by optical rectification," *Opt. Exp.*, vol. 13, pp. 5762–5768, 2005.

[16] J.-I. Shikata, M. Sato, T. Taniuchi, H. Ito, and K. Kawase, "Enhancement of terahertz-wave output from LiNbO₃ optical parametric oscillators by cryogenic cooling," *Opt. Lett.*, vol. 24, pp. 202–204, 1999.

[17] G. Gallot, J. Zhang, R. W. McGowan, T.-I. Jeon, and D. Grischkowsky, "Measurements of the THz absorption and dispersion of ZnTe and their relevance to the electro-optic detection of THz radiation," *Appl. Phys. Lett.*, vol. 74, pp. 3450–3452, 1999.

[18] P. H. Siegel, "Terahertz technology," *IEEE Trans. Microw. Theory Tech.*, vol. 50, no. 3, pp. 910–928, Mar. 2002.

[19] T. J. Carrig, G. Rodriguez, T. S. Clement, and A. J. Taylor, "Scaling of terahertz radiation via optical rectification in electro-optic crystals," *Appl. Phys. Lett.*, vol. 66, pp. 121–123, 1995.

[20] Y.-S. Lee, T. Meade, M. DeCamp, T. B. Norris, and A. Galvanauskas, "Temperature dependence of narrow-band terahertz generation from periodically poled lithium niobate," *Appl. Phys. Lett.*, vol. 77, pp. 1244–1246, 2000.

[21] K. L. Vodopyanov, M. M. Fejer, X. Yu, J. S. Harris, Y.-S. Lee, W. C. Hurlbut, V. G. Kozlov, D. Bliss, and C. Lynch, "Terahertz-wave generation in quasi-phase-matched GaAs," *Appl. Phys. Lett.*, vol. 89, pp. 141119-1–141119-3, 2006.

[22] G. Imeshev, M. E. Fermann, K. L. Vodopyanov, M. M. Fejer, X. Yu, J. S. Harris, D. Bliss, and C. Lynch, "High-power source of THz radiation based on orientation-patterned GaAs pumped by a fiber laser," *Opt. Exp.*, vol. 14, pp. 4439–4444, 2006.

[23] E. D. Palik, *Handbook of Optical Constants of Solids,* vol. I. New York: Academic, 1985, pp. 409–427, 429–443, and 695–702.

[24] E. D. Palik, *Handbook of Optical Constants of Solids,* vol. II. New York: Academic, 1991, pp. 559–578 and 737–758.

[25] L. A. Gordon, G. L. Woods, R. C. Eckardt, R. R. Route, R. S. Feigelson, M. M. Fejer, and R. L. Byer, "Diffusion-bonded stacked GaAs for quasi-phase-matched second-harmonic generation of a carbon dioxide laser," *Electron. Lett.*, vol. 29, pp. 1942–1944, 1993.

[26] L. A. Eyres, P. J. Tourreau, T. J. Pinguet, C. B. Ebert, J. S. Harris, M. M. Fejer, L. Becouarn, B. Gerard, and E. Lallier, "All-epitaxial fabrication of thick, orientation-patterned GaAs films for nonlinear optical frequency conversion," *Appl. Phys. Lett.*, vol. 79, pp. 904–906, 2001.

[27] K. L. Vodopyanov, "Optical generation of narrow-band terahertz packets in periodically-inverted electro-optic crystals: Conversion efficiency and optimal laser pulse format," *Opt. Exp.*, vol. 14, pp. 2263–2276, 2006.

[28] E. C. Cheung, K. Koch, and G. T. Moore, "Frequency upconversion by phase-matched sum-frequency generation in an optical parametric oscillator," *Opt. Lett.*, vol. 23, pp. 1967–1969, 1994.

[29] M. E. Dearborn, K. Koch, G. T. Moore, and J. C. Diels, "Greater than 100% photon-conversion efficiency from an optical parametric oscillator with intracavity difference-frequency mixing," *Opt. Lett.*, vol. 23, pp. 759–761, 1998.

[30] T. Skauli, P. S. Kuo, K. L. Vodopyanov, T. J. Pinguet, O. Levi, L. A. Eyres, J. S. Harris, M. M. Fejer, B. Gerard, L. Becouarn, and E. Lallier, "Improved dispersion relations for GaAs and applications to nonlinear optics," *J. Appl. Phys.*, vol. 94, pp. 6447–6455, 2003.

[31] D. Grischkowsky, S. Keiding, M. Exter, and Ch. Fattinger, "Far-infrared time-domain spectroscopy with terahertz beams of dielectrics and semiconductors," *J. Opt. Soc. Amer. B*, vol. 7, pp. 2006–2015, 1990.

[32] R. H. Stolen, "Far-infrared absorption in high resistivity GaAs," *Appl. Phys. Lett.*, vol. 15, pp. 74–75, 1969.

[33] J. S. Blakemore, "Semiconducting and other major properties of gallium arsenide," *J. Appl. Phys.*, vol. 53, pp. R132–R181, 1982.

[34] C. Lynch, D. Bliss, T. Zens, V. Tassev, P. Kuo, A. Lin, J. Harris, M. Fejer, and P. Schunemann, "mm-thick orientation-patterned GaAs for IR and THz generation," presented at the 15th Int. Conf. Crystal Growth, Session: Crystal Growth Laser Host NLO Crystals, Salt Lake City, UT, 2007.

[35] P. Kuo, K. Vodopyanov, A. Markosyan, A. Alexandrovski, M. Fejer, X. Yu, A. Lin, J. Harris, D. Bliss, C. Lynch, T. Zens, and D. Weyburne, "Orientation-patterned gaas for generation of mid-infrared radiation," presented at the 15th Int. Conf. Crystal Growth, Session: Crystal Growth Laser Host NLO Crystals, Salt Lake City, UT, 2007.

[36] D. A. Roberts, "Simplified characterization of uniaxial and biaxial nonlinear optical crystals: A plea for standardization of nomenclature and conventions," *IEEE J. Quantum Electron.*, vol. 28, pp. 2057–2073, 1992.

[37] M. M. Choy and R. L. Byer, "Accurate second-order susceptibility measurements of visible and infrared nonlinear crystals," *Phys. Rev. B*, vol. 14, pp. 1693–1706, 1976.

[38] J. E. Schaar, K. L. Vodopyanov, and M. M. Fejer, "Intracavity terahertz-wave generation in a synchronously pumped optical parametric oscillator using quasi-phase-matched GaAs," *Opt. Lett.*, vol. 32, pp. 1284–1286, 2007.

[39] K. L. Vodopyanov, J. E. Schaar, P. S. Kuo, M. M. Fejer, X. Yu, J. S. Harris, V. G. Kozlov, D. Bliss, and C. Lynch, "Terahertz wave generation in orientation-patterned GaAs using resonantly enhanced scheme," *Proc. SPIE*, vol. 6455, p. 645509 1–9, 2007.

[40] R. Paschotta, J. A. der Au, and U. Keller, "Thermal effects in high-power end-pumped lasers with elliptical-mode geometry," *IEEE J. Sel. Topics Quantum Electron.*, vol. 6, no. 4, pp. 636–642, Jul./Aug. 2000.

[41] A. Yariv and P. Yeh, *Optical Waves in Crystals: Propagation and Control of Laser Radiation*. New York: Wiley, 1984, pp. 511–512.

[42] L. E. Myers and W. R. Bosenberg, "Periodically poled lithium niobate and quasi-phase-matched optical parametric oscillators," *IEEE J. Quantum Electron.*, vol. 33, no. 10, pp. 1663–1672, Oct. 1997.

[43] M. Cronin-Golomb, "Cascaded nonlinear difference-frequency generation enhanced terahertz wave production," *Opt. Lett.*, vol. 29, pp. 2046–2048, 2004.

[44] K.-L. Yeh, M. C. Hoffmann, J. Hebling, and K. A. Nelson, "Generation of 10 μJ ultrashort terahertz pulses by optical rectification," *Appl. Phys. Lett.*, vol. 90, pp. 171121-1–171121-3, 2007.

[45] A. E. Siegman, "Nonlinear optical effects: An optical power limiter," *Appl. Opt.*, vol. 1, pp. 739–744, 1962.

[46] R. C. Eckardt, C. D. Nabors, W. J. Kozlovsky, and R. L. Byer, "Optical parametric oscillator frequency tuning and control," *J. Opt. Soc. Amer. B*, vol. 8, pp. 646–667, 1991.

[47] A. Douillet, J.-J. Zondy, A. Yelisseyev, S. Lobanov, and L. Isaenko, "Stability and frequency tuning of thermally loaded continuous-wave AgGaS₂ optical parametric oscillators," *J. Opt. Soc. Amer. B.*, vol. 16, pp. 1481–1498, 1999.

Joseph E. Schaar received the B.S. degree in electrical engineering from the University of Arizona, Tucson, in 2003, the M.S. degree in electrical engineering from Stanford University, Stanford, CA, in 2005, where he is currently working toward the Ph.D. degree in electrical engineering at the E. L. Ginzton Laboratory.

His current research interests include terahertz-wave generation in quasi-phase-matched GaAs using intracavity parametric down-conversion, doubly resonant optical parametric oscillator stabilization techniques, and synchronously pumped OPO modeling.

Mr. Schaar is a member of the Optical Society of America (OSA).

Konstantin L. Vodopyanov received the Master's degree from Moscow Phys-Tech, Moscow, Russia, in 1976, the Ph.D. degree from the Oscillations Laboratory, Lebedev Physical Institute, Moscow, in 1983, and the D.Sc. degree (Habilitation) from the General Physics Institute, Moscow, in 1993.

During 1985–1990, he was an Assistant Professor at Moscow Phys-Tech, during 1990–1992, a Alexander-von-Humboldt Fellow at the University of Bayreuth, Germany, and during 1992–1998, a Lecturer at the Imperial College, London, U.K. During 1998–2000, he was the Head of the Laser Group, Inrad, Inc., NJ, and later, during 2000–2003, the Director of mid-IR systems at Picarro, Inc., CA. In 2003, he returned to Academia and is now at the Edward L. Ginzton Laboratory, Stanford University, Stanford, CA. His current research interests include laser interaction with matter, laser spectroscopy, nonlinear optics, mid-IR and terahertz-wave generation using micro- and nanostructured materials, as well as spectrally resolved atomic force microscopy.

Dr. Vodopyanov was a Fellow of the Royal Society during 1992–1998. He was elected as a Fellow of the U.K. Institute of Physics in 1997 and Optical Society of America in 1998. He is a member of program committees for several major laser conferences and has been elected as the Program Chair for the Conference on Lasers and Electro-Optics (CLEO) 2008 and the General Chair for CLEO 2010.

Paulina S. Kuo received the B.S. degrees in physics and materials science from the Massachusetts Institute of Technology, Cambridge, in 2000. She is currently working toward the Ph.D. degree in applied physics from Stanford University, Stanford, CA.

Ms. Kuo is a member of the Optical Society of America (OSA) and the Society of Photo-optical Instrumentation Engineers (SPIE).

Martin M. Fejer (M'93) received the B.A. degree in physics from Cornell University, Ithaca, NY, in 1977, and the M.S. and Ph.D. degrees in applied physics from Stanford University, Stanford, CA, in 1979 and 1986, respectively.

In 1986, he joined the faculty at Stanford, where he is currently a Professor of Applied Physics. He is the author or coauthor of more than 200 technical publications. He holds 20 patents. His current research interests include nonlinear optical materials and devices, guided wave optics, microstructured ferroelectrics and semiconductors, nonlinear devices for telecommunications applications, low dissipation materials, and precision measurements.

Prof. Fejer is a Fellow of the Optical Society of America (OSA) and a member of the IEEE LEOS Board of Governors. He is also a member of the American Association for Crystal Growth (AACG) and the Society of Photo-optical Instrumentation Engineers (SPIE).

In 1998, he was the recipient of the Optical Society of America (OSA) R.W. Wood Prize.

Xiaojun Yu received the B.S. and M.S. degrees in materials science and engineering from Tsinghua University, Beijing, China, in 1998 and 2000, respectively, and the second M.S. degree in electrical engineering and the Ph.D. degree in materials science and engineering from Stanford University, Stanford, CA, in 2004 and 2006, respectively.

He was engaged in research in the area of molecular beam epitaxy and the applications in nonlinear optics. From 2005 to 2006, he was with Micron Technology, where he was engaged in research on nonvolatile NOT–AND circuit (NAND) flash memory design. In 2006, he joined IBM Semiconductor Research and Development Center, East Fishkill, NY.

Angie Lin is currently working toward the Ph.D. degree in materials science and engineering at Stanford University, Stanford, CA.

Her current research interests include molecular beam epitaxial growth of two different materials systems, GaAs-Ge and GaP-Si, and development of orientation-patterned GaP structures for nonlinear optical applications.

James S. Harris, photograph and biography not available at time of publication.

David Bliss received the B.A. degree in economics from Case-Western Reserve University, Clevend, OH, in 1968 the S.M. degree in engineering (materials science) from the Massachusetts Institute of Technology, Cambridge, in 1981, and the Ph.D. degree in materials science from State University of New York (SUNY) Stony Brook, in 2000.

He is a Program Manager of substrate engineering and crystal growth in the Optoelectronic Technology Branch of the Air Force Research Laboratory at Hanscom Air Force Base, MA.

Dr. Bliss is a member, Executive Committee Member, and President of the American Associtaion for Crystal Growth. He is a member of the Crystal Growth Commission and the International Union of Crystallography.

Candace Lynch received the S.B. degree from the Massachusetts Institute of Technology, Cambridge, in 1999, and the Ph.D. degree from Brown University, Providence, RI, in 2004, both in engineering (materials science).

She was engaged in research on *in situ* measurement of strain relaxation during lattice mismatched epitaxial growth of III-arsenides. From January 2005 to February 2007, she was a National Research Council Postdoctoral Research Associate at the Air Force Research Laboratory (AFRL), Hanscom Air Force Base, Bedford, MA. Since February 2007, she has been a Research Physicist with the AFRL. Her current research interests include hydride vapor phase epitaxial growth of thick layers for nonlinear optical frequency conversion.

Vladimir G. Kozlov received the M.S. degree in physics from Moscow State University, Moscow, Russia, in 1992, and the Ph.D. degree in physics from Brown University, Providence, RI, in 1997.

He held research positions at Lucent Technologies and Princeton University. He is the Vice President of Microtech Instruments, Inc., Eugene, OR. He has more than 20 years of experience in research and development of optoelectronic systems, including terahertz (THz) devices.

Walter Hurlbut, photograph and biography not available at time of publication.